

Stable Cone Notes

S.D. Ellis¹

¹U of W, Seattle, WA 98195 USA

(Dated: September 4, 2002)

We discuss recent progress in understanding the issues essential to improving cone jet algorithms.

In these notes we want to address the question of when two nearby energetic partons are included in a single jet. We will include both the effects of the details of the jet algorithm and the effects of the showering and hadronization that bridge the logical gap between fixed order perturbative results and real data (and MC data). The goal, of course, is to understand enough of the details to be able to understand the history of jets physics and to design an algorithm that minimized the dependence on these nonperturbative effects.

In the lowest order description of large E_T jet production in hadronic collisions, we find just two jets in the final state and just one energetic parton per jet. The only questions are how much energy is lost to the final jet due to the smearing effects of showering and hadronization (“splash-out”) and how much extra energy “leaks” into the jet from the parts of the initial and final state interactions not directly associated with the hard scattering (“splash-in”). These are expected to be relatively small effects compared to what we will discuss below, although we are focused on issues relevant for precision of better than 10%. At NLO the extra parton can lead to either an extra jet or to a second parton in one of the first two jets. It is exactly the question of how to separate these two situations that we will discuss here. It is essential to recognize that there is no first principles “right answer” to this question. The boundary between the 2-jet configuration and the “fat-jet” configuration is clearly arbitrary. On the other hand, it is important (at the 5 to 10% level) that the boundary be robust in moving from the perturbative analysis to the experimental analysis, *i.e.*, the boundary should be insensitive to the effects of showering and hadronization.

We begin by considering the original Snowmass Accord definition of the cone algorithm. The cone jet defines nearness in an intuitive geometric fashion: jets are composed of hadrons or partons whose 3-momenta lie within a cone defined by a circle in (η, ϕ) . These are the usual angular variables, where $\eta = \ln(\cot \theta/2)$ is the pseudorapidity and ϕ is the azimuthal angle. We also expect the jets to be aligned with the most energetic particles in the final state. This expectation is realized in the Snowmass Algorithm by defining an acceptable jet in terms of a “stable” cone such that the geometric center of the cone is identical to the E_T weighted centroid. Thus, if we think of a sum over final state partons or hadrons defined by an index k and in the direction (η_k, ϕ_k) , a jet (J) of cone radius R is defined by the following set of equations

$$\begin{aligned}
 k \in J : (\phi_k - \phi_J)^2 + (\eta_k - \eta_J)^2 &\leq R^2, \\
 \phi_J = \bar{\phi}_J &\equiv \sum_{k \in J} \frac{E_{T,k} \phi_k}{E_{T,J}}, \quad \eta_J = \bar{\eta}_J \equiv \sum_{k \in J} \frac{E_{T,k} \eta_k}{E_{T,J}}, \\
 E_{T,J} &= \sum_{k \in J} E_{T,k}.
 \end{aligned} \tag{1}$$

In these expressions E_T is the transverse energy ($|\vec{p}_T|$ for a massless 4-vector). It is important to recognize that jet algorithms involve two distinct steps. The first step is to identify the “members” of the jet, *i.e.*, the calorimeter towers or the partons that make-up the stable cone that becomes the jet. The second step involves constructing the kinematic properties that will characterize the jet, *i.e.*, determine into which bin the jet will be placed. In the original Snowmass Algorithm the E_T weighted variables defined in Eq. 1 are used both to identify and bin the jet. As simple as the cone idea sounds, its implementation has involved several compromises that we wish to illuminate in these notes. As a laboratory for our studies we consider a simply 2-parton configuration, where the partons are separated in (η, ϕ) space by a distance d and the ratio of energies is $z = E_{T,2}/E_{T,1}$, where $E_{T,2} \leq E_{T,1}$. We can visualize the corresponding E_T distribution, *i.e.*, 2 delta functions, as indicated in Fig. 1.

If we apply the Snowmass Algorithm to the 2-parton configuration, we can subdivide the (z, d) phase space according to the number of stable cones with the results, for the canonical value $R = 0.7$, indicated in Fig. 2. We interpret this figure to mean that, for $d \leq R$ with any value of z , the cone algorithm finds a single stable cone containing both partons and located at the position of the E_T weighted centroid (hence the subscript C on the 1). In the region $R < d \leq R(1+z)$ the algorithm identifies 3 stable cones, one centered on the left-most parton (the parton at the “origin”) that does not include the right-most parton, one centered on the right-most parton (the parton at d) that does not include the left-most parton, and the central stable cone that includes both partons and is centered between the partons at the E_T weighted centroid (again as suggested by

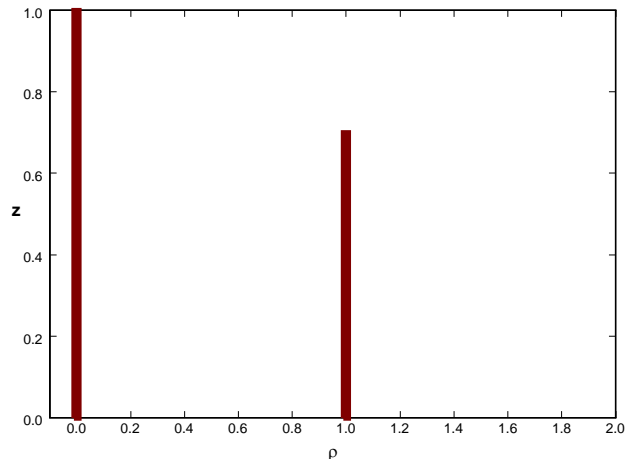


FIG. 1: Two parton E_T distribution for $d = 1$, $z = 0.7$, where ρ is the separation in (η, ϕ) .

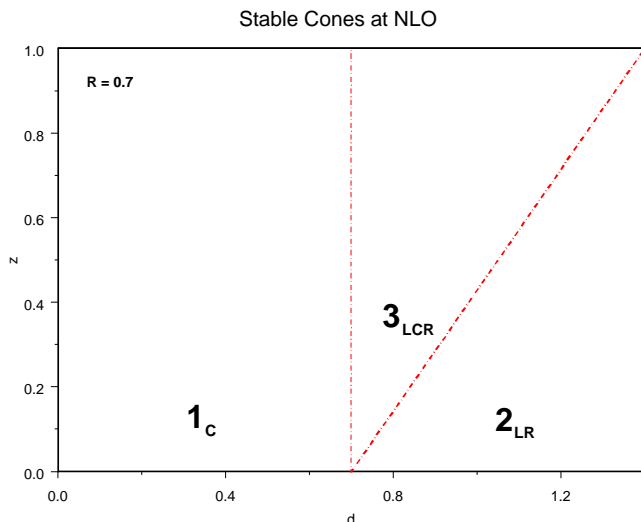


FIG. 2: 2-parton phase space in NLO.

the subscript on the 3). Finally to the right ($d > R(1 + z)$) the Snowmass algorithm finds just 2 stable cones, one centered on each of the partons. (For reference we will keep this boundaries in subsequent graphs.)

To determine the location of the stable cones we can consider the “Snowmass potential” defined by a sum over the partons (or calorimeter towers and particles) contained within the cone C of radius R

$$V_{\text{Snowmass}}(r) = -\frac{1}{2} \sum_{k \in C(r)} E_{T,k} \times \left(R^2 - (\vec{\rho}_k - \vec{r})^2 \right) \times \Theta \left(R^2 - (\vec{\rho}_k - \vec{r})^2 \right), \quad (2)$$

$$k \in C(r) \text{ iff } (\vec{\rho}_k - \vec{r})^2 \leq R^2.$$

The gradient of this function, the “Snowmass force”, vanishes at the locations of the stable cones of Eq. 1. Thus the extrema of the potential correspond to the desired stable cones. If we evaluate the Snowmass potential for the distribution of Fig. 1 in the 3_{LCR} region of Fig. 2 we find the function plotted in Fig. 3. The three minima, corresponding to the three stable cones in the locations noted, are clearly visible.

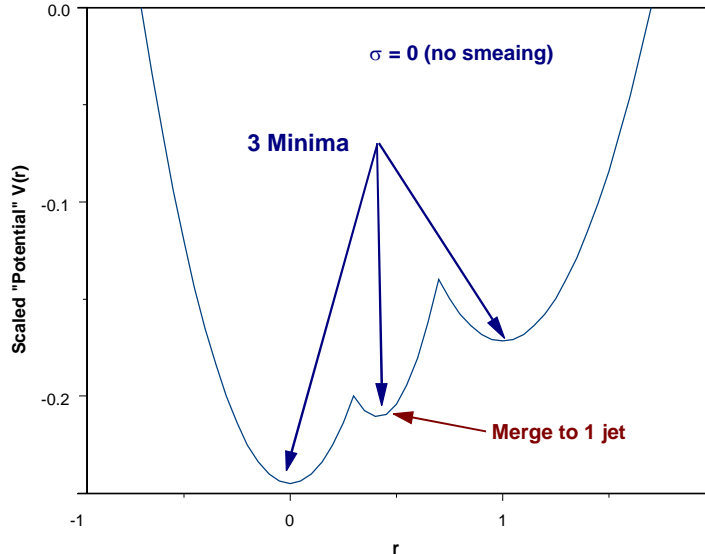


FIG. 3: Snowmass potential for $d = 1$, $z = 0.7$.

So the question arises, will this structure be apparent in analyzes of real data? Several sorts of issues keep life from being this simple. First, as we shall discuss shortly, the actual experimental implementation of the Snowmass algorithms is more complicated than implied above. Secondly, the real physics of parton showering (the all orders inclusion of the singular collinear structure of QCD) and hadronization (partons confined to the final state hadrons) intervenes to somewhat smear the true E_T distribution, to which the algorithm is applied. Consider first the issue of overlapping stable cones, a point not directly addressed in the Snowmass Accord but already apparent in Fig. 3. While the stable cones at $r = 0$ and $r = d = 1.0$ are distinct (sharing no E_T), the central stable cone at $r \simeq 0.4$, in fact, overlaps with both of the other two stable cones, sharing 100% of their E_T . In the NLO calculations of EKS only the central cone was kept on the grounds that this was obviously the correct choice with such 100% overlap. In the experimental case with real data where the E_T is smeared out, the situation is less clear and explicit rules for merging/splitting of overlapping stable cones were developed. After finding the stable cones, overlapping pairs were studied in order beginning with those with the largest E_T . We define $E_{T,1}$ and $E_{T,2}$ as the E_T values in each cone, with $E_{T,2} < E_{T,1}$, and $E_{T,\text{overlap}}$ as the total E_T in the region of overlap. Then the question of how to proceed is defined by a single parameter f_{merge} (in Run I $f_{\text{merge}} = 0.75$ for CDF and $f_{\text{merge}} = 0.5$ for DØ). If $E_{T,\text{overlap}}/E_{T,2} \geq f_{\text{merge}}$, then the two stable cones are merged to form *i.e.*, all partons (or calorimeter towers and charged particles) are included in, the final jet. In the case that $E_{T,\text{overlap}}/E_{T,2} < f_{\text{merge}}$, the partons (or calorimeter towers and charged particles) in the overlap region are split between two jets (one for each stable cone) according to which cone center is closer. Thus in the NLO situation the merging/splitting rule specifies that the 3 stable cones are merged into a single jet, just as in the EKS calculations, independent of the specific value of f_{merge} , since the overlap is 100%. Note that these merging/splitting rule will have no impact at NLO on the 2_{LR} region as there is no E_T in the overlap region. This situation can change when more realistic smearing (showering and hadronization) are included. The resulting “found jet” content looks as in Fig. 4, where the subscripts again specify the location of the final, either at one of the partons (L or R) or central including both partons.

The preceding discussion assumes that all 3 stable cones are, in fact, identified by the application of the Snowmass algorithm. While in the perturbative calculation it is straightforward to find *all* stable cones by construction, the application to real data has typically involved efforts to simplify the analysis through the employment of “seeds”. The idea is to identify locations in (η, ϕ) (*e.g.*, calorimeter towers) that are likely to be near the center of a jet by using a minimum E_T cut (the E_T in the tower). Then at the location of each of these seeds we put the center of a trial cone. Using the expressions in Eq. 1 we calculate the centroid for the calorimeter towers within this cone. If the centroid is distinct from the original seed location, we move the cone center to this centroid and calculate the centroid corresponding to this new cone location. This process is iterated until the location of the trial cone is stable, *i.e.*, the centroid coincides with geometric center. In the

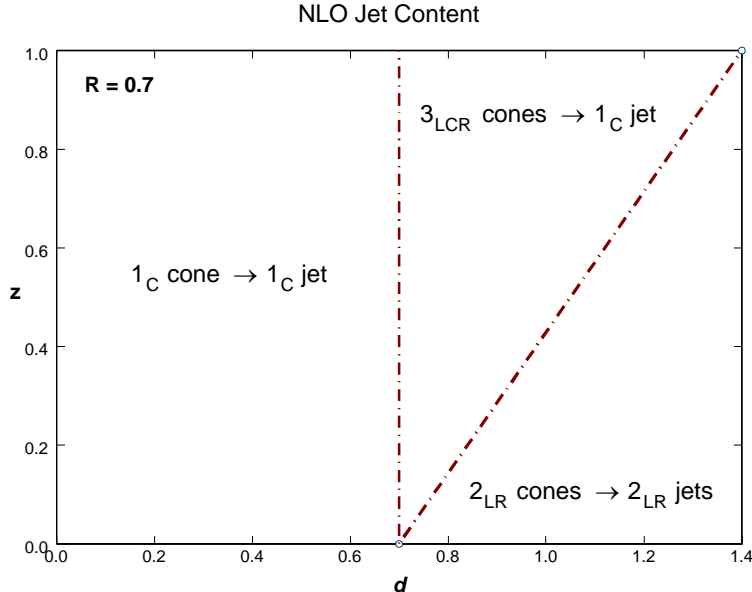


FIG. 4: NLO jet content.

language suggested by Eq. 2 and Fig. 3, if we put a seed near one of the minima of the Snowmass potential, the Snowmass force will push the trial cone to the nearest minima (*i.e.*, on iteration the trial cone will migrate to the local minima). So to connect to the NLO results, we must determine where the seeds are likely to be. Clearly there will be seeds near the locations of the partons (0 and d) and we can expect that the experimental analysis will identify the \mathbf{L} and \mathbf{R} stable cones, if they exist. On the other hand, since the region between the original partons may be of low E_T even in the real world (there is no E_T at NLO), there may be no seed near the the central stable cone. Thus it is possible for the experimental application of the Snowmass algorithm to miss the central stable cone that is found by the perturbative application of the algorithm in the region of Fig. 2 labeled by 3_{LCR} (after merging) due to the absence of a central seed. It was concern about this issue that first led to the inclusion of the *ad hoc* parameter R_{sep} to simulate the impact of seeds in the theoretical analysis. It was assumed that for large separation ($d > R * R_{sep}$) the experimental, and therefore the theoretical analysis will not identify the central stable cone (because there is not enough central E_T activity to generate a seed). The corresponding version of Fig. 2 looks like Fig. 5. The value $R_{sep} = 1.3$ is chosen to provide reasonable agreement with the data (both CDF and DØ have “certified” this value).

The final issue to be included is the impact of nonperturbative smearing (showering and hadronization) on the shape of the Snowmass potential, *i.e.*, on the location, and even existence, of the stable cones. In the analytic studies to be summarized here, we simulated the effects of showering and hadronization by smearing the delta functions of Fig. 1 with a Gaussian smearing function of width σ for the specific values $\sigma = 0.1$ and 0.25 (the smearing occurs in the 2-D angular variable $r = (\eta, \phi)$). We will also exhibit results from smearing using an E_T profile derived by DØ from fitting the profile inside jets with $R = 1.0$.

With Gaussian smearing included with $\sigma = 0.1$ the underlying E_T distribution of Fig. 1 now looks like The smearing of the underlying E_T distribution will result in “smearing” of the Snowmass potential leading to a displacement and even disappearance of stable cones. For example, with $\sigma = 0.1$, $z = 0.7$ and $d = 1.0$ (as above) the Snowmass potential is illustrated in Fig. 7 where we note that the central stable cone has been “washed out” by the smearing. With even more smearing, $\sigma = 0.25$, as in Fig. 8, we see that the right-most stable cone has also been washed out. These changes in the stable cone content can be summarized in the analogues of Fig. 2, illustrated in Fig. 9 and Fig. 10. In these plots the dashed line represents the “soft” boundary between the single stable cone in the central position to the single stable cone over the left-most parton (the location of the stable cone simple migrates smoothly to the left as d increases). As expected the region in (d, z) where there were initially 3 stable cones is partially converted into regions with no right-most stable cone (the 2_{LC} region), no central or right-most stable cone (the 1_{L} region) and no central stable cone (the enlarged 2_{LR} region). If we further assume that there is no central seed in the remaining 3_{LCR} region, this region is effectively added to the

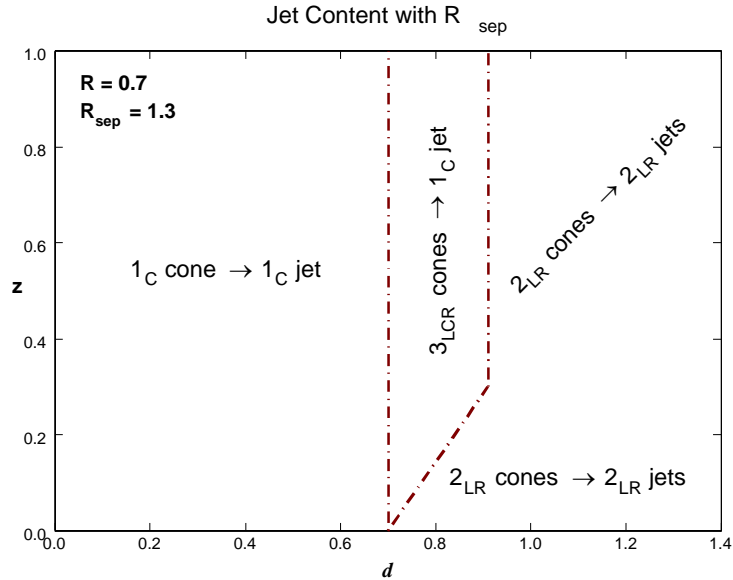


FIG. 5: The (d, z) phase space jet content with the parameter R_{sep} included.

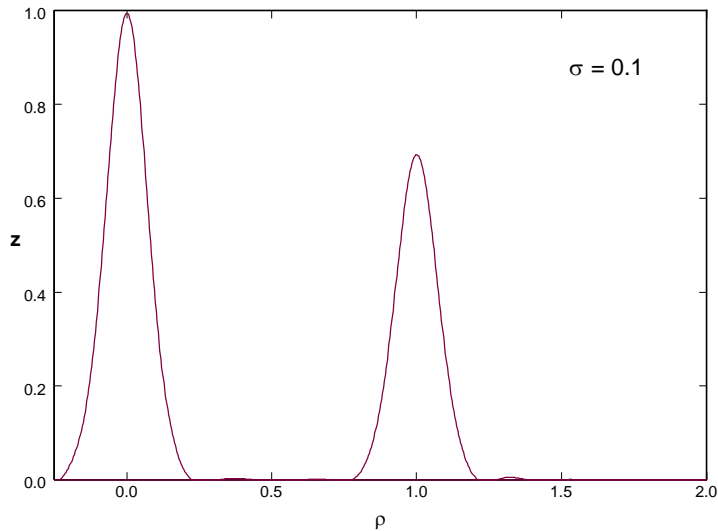


FIG. 6: E_T distribution with $\sigma = 0.1$ Gaussian smearing.

2_{LR} region. Note on the other hand, that the 2_{LC} region will still produce a central stable cone as this stable cone is “seeded” by the right-most parton. There is no stable cone at the right position to keep the trial cone from migrating to the center. Thus, compared to NLO, for both values of σ we lose the central stable cone for $z > (d - R)/R$ and $d \gtrsim 0.85$, or $R_{sep} \approx 1.2$ (*i.e.*, only the regions 1_C and 2_{LC} produce central stable cones and merged jets). Note also that in the region $z < (d - R)/R$ and $d \gtrsim 0.85$ we have also lost the right-hand, *i.e.*, lower E_T , stable cone (and thus the lower E_T second jet). This is the region of Matthias’ “lost jets”, which will be more relevant when we discuss ratcheting below.

Since this Gaussian smearing model may not provide a faithful description of the real smearing due to

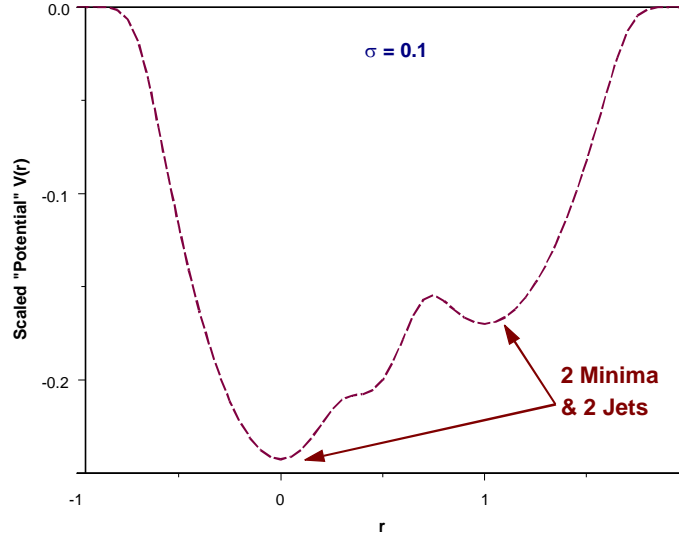


FIG. 7: Snowmass potential with Gaussian smearing, $\sigma = 0.1$.

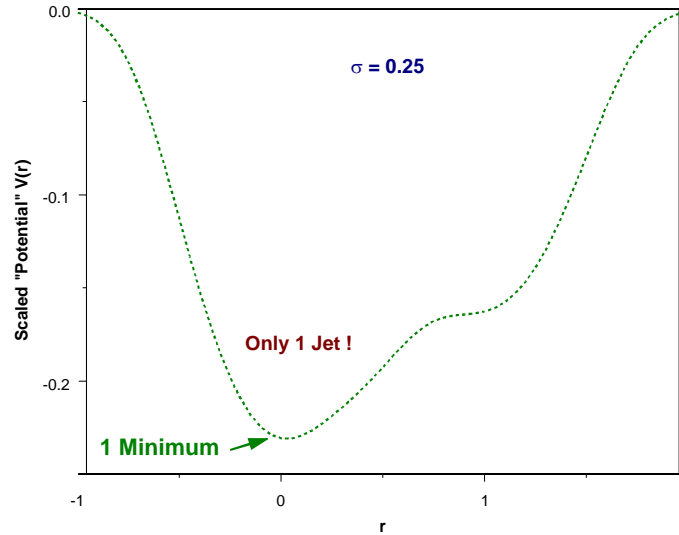
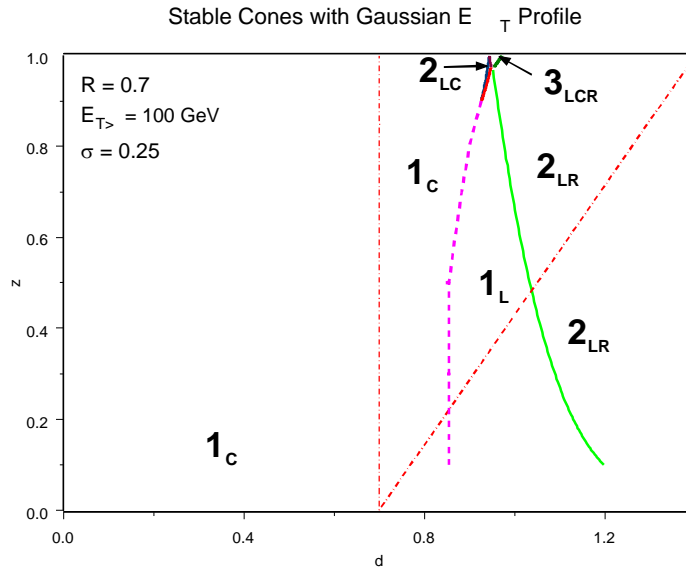
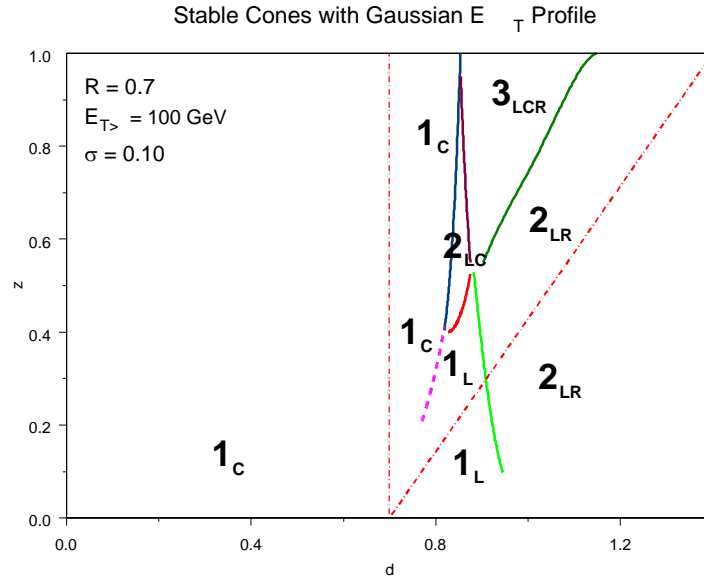


FIG. 8: Snowmass potential with Gaussian smearing, $\sigma = 0.25$.

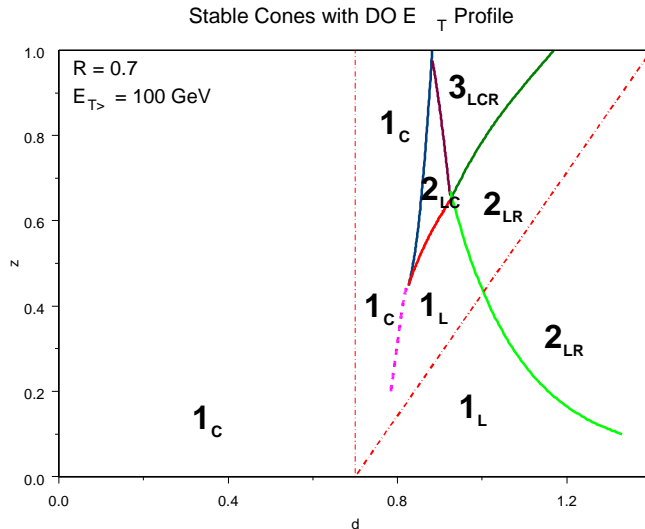
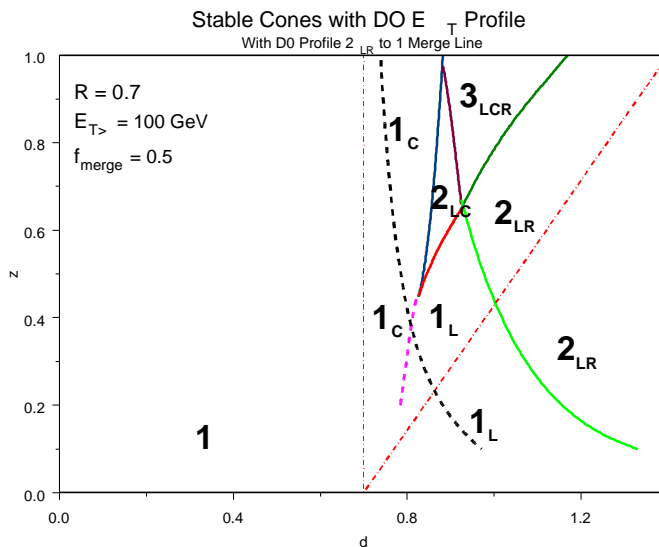
showering and hadronization (in any case we are studying only the average behavior with not fluctuating component), we perform the same analysis with a smearing profile equal to the $D\emptyset$ fit to their only internal jet profiles with $R = 1.0$. Using this as a model of how the partonic E_T is smeared out by showering and hadronization, we arrive the stable cone structure illustrated in Fig. 11, which we note is quite similar to the Gaussian $\sigma = 0.1$ result. Since $D\emptyset$ has used this profile to argue for the value $R_{sep} = 1.3$ by studying how far apart two cones with this internal E_T profile must be in order not to be merged by the merging/splitting rule, Fig. 12 is the same as the Fig. 11, but with the calculated merge boundary also displayed (with the $D\emptyset$ value $f_{merge} = 0.5$). We see that the merging process is unlikely to play a role in the 2_{LR} region. (Note that my results suggest a less important role for merging than those in the $D\emptyset$ analysis. I produce the results in the



DØ note only in I include an arbitrary factor of 2 in the calculation of the energy in the overlap region.)

To summarize the preceding discussion we see that, compared to the NLO results, the experimental versions of the Snowmass algorithm can miss the merged central stable cone for several reasons:

- There is no central seed;
- There is no central stable cone (due to the smearing effects of showering and hadronization);
- There is not enough overlap to result in merging by the merging/splitting rule.

FIG. 11: Stable cones using the $D\bar{O}$ E_T profile.FIG. 12: Stable cones using the $D\bar{O}$ E_T profile with 2_{LR} to 1 merge boundary indicated.

The second reason is likely to be as important as the first, while the third reason seems to play little role (especially with no central seeds). Note that while the MidPoint algorithm is designed to address the first issue (by explicitly adding a seed between every nearby pair of stable cones), it will not help if smearing has washed out the central stable cone (the second issue). Due to the smearing effects we have also lost secondary, low E_T jets in the region where, in fact, the rate is large due to the combined infrared and collinear singularities in QCD (i.e., z small and $d \gtrsim R$). However, since these are secondary jets, the numerical impact on the jet cross section is small relative to NLO (i.e., they occur at the small rate characterized by the larger E_T primary jets and their contribution is suppressed by the fact that the cross section falls rapidly with E_T). These comments should be relevant to the Run I algorithm used by $D\bar{O}$.

To discuss the CDF jet results we need to include the special feature of JETCLU - ratcheting. This feature ensures that as the trial cone migrates away from the initial seed position, any calorimeter tower included in the initial trial cone stays with trial “cone” (“once in a cone, always in a cone”), which is no longer cone

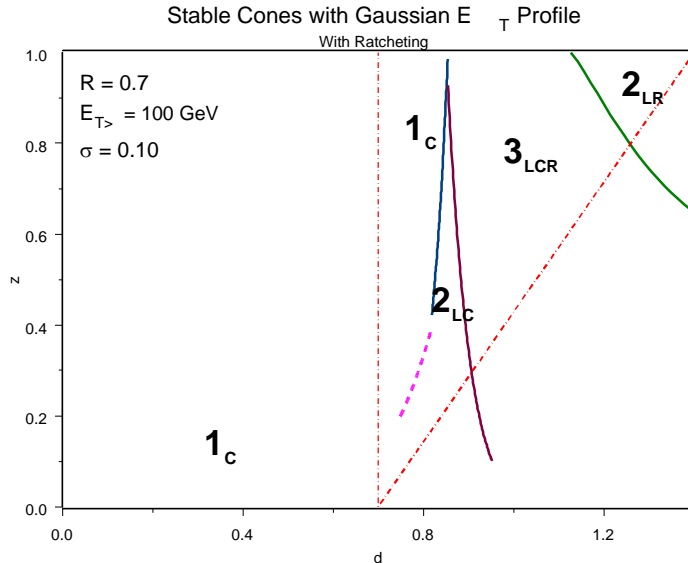


FIG. 13: Gaussian smearing, $\sigma = 0.1$, with ratcheting.

shaped . Thus with ratcheting turned on the “history” of a migrating trial cone matters. The lists of towers to be summed over in Eqs. 1 and 2 grow with migration and a tower k no longer needs to be within R of the cone center to be included. In the current analysis we can define the integral (the potential) over the smeared E_T profiles to take this ratcheting into account, with two distinct potentials depending on whether we are “seeded” by the left-most or right-most parton. The stable cones are then the sum of the stable cones found from both potentials. In general, the central stable cones identified by the two potentials (if present) are nearly coincident. On the other hand, the right-hand potential will not exhibit a left-hand stable cone - due to ratcheting, it cannot migrate that far - and vice versa. With smearing present the left-hand potential will tend to have only a left-hand stable cone, while the right-hand potential will tend to have only a central stable cone (and not just a right-hand stable cone as it did in the non-ratcheted case above). The analogues of the stable cone structures above but now with ratcheting present are exhibited in the next 3 graphs, Figs. 9, 10 and 11. We see from these figures that the impact of ratcheting is to greatly expand the 2_{LC} and 3_{LCR} regions at the expense of the (undesirable) 1_L and 2_{LR} regions. Of particular importance is the appearance of a large region below the line $z = (d - R)/R$ that is now of type 2_{LC} , instead of 1_L (or even 2_{LR} as it was at NLO). This implies that in this region, where the cross section is large, we will identify a central stable cone and thus a merged jet (encompassing both partons) using the experimental algorithm on data, while the theoretical NLO results identifies two distinct, non-merged jets. Since this merging has the effect of increasing the E_T of the primary jet in the event, the numerical impact compared to NLO is enhanced by the fact that the cross section falls rapidly with E_T and can be sizable, $\sim 5 - 10\%$.

In an effort to summarize what we have discussed, the following figures illustrate the jet content of the stable cone graphs above for the case of the $D\emptyset$ E_T profile. For the generic cone (“ $D\emptyset$ -like”) algorithm, assuming that there are no seeds in the central region (so that 3_{LCR} yields two distinct jets, 2_{LR}) we have Fig. 16. If we consider the same situation but with the MidPoint algorithm so that we explicitly place a seed between pairs of stable cones, we will identify the 3_{LCR} case as a 1_C jet and the new graph is the in Fig. 17. Now we have “reclaimed” as a merged jet the large z region for $0.9 \lesssim d \lesssim 1.1$. As attractive as this change is in our quest to reproduce NLO, there are very few events in this region of phase space (neither soft nor collinear emissions) and the numerical impact of the MidPoint algorithm. More important numerically is the 1_L region just above the line $z = (d - R)/R$, where the rate is larger and where, compared to NLO, a 1_C configuration has become 1_L . The jets in this region will involve only the larger E_T parton and thus have lower E_T relative to the NLO central jet with both partons. This also can lead to the “lost” secondary jets noted by Matthias, the secondary parton is neither merged in a primary jet not included in a secondary jet by itself. Note that this region is unchanged by the seed issue or the MidPoint algorithm. (If Krane is comparing the MidPoint algorithm with the $D\emptyset$ algorithm, he should not see a “lost” jet effect.)

In Fig. 18 we see the corresponding version for the CDF JETCLU algorithm with ratcheting. The large

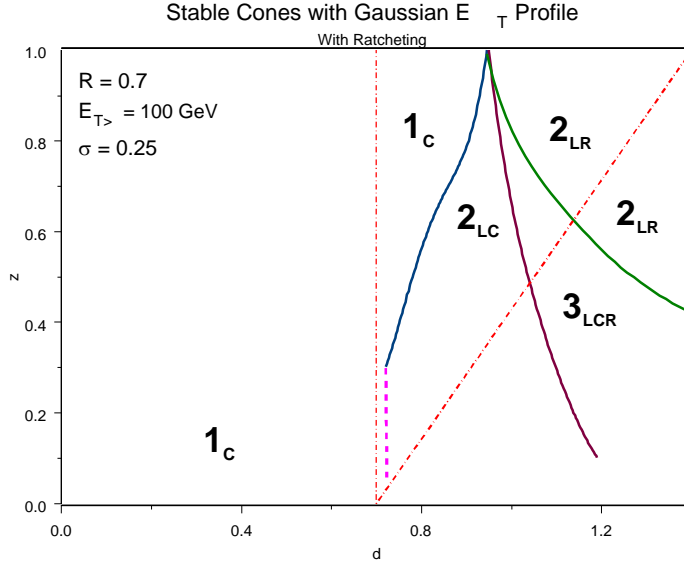
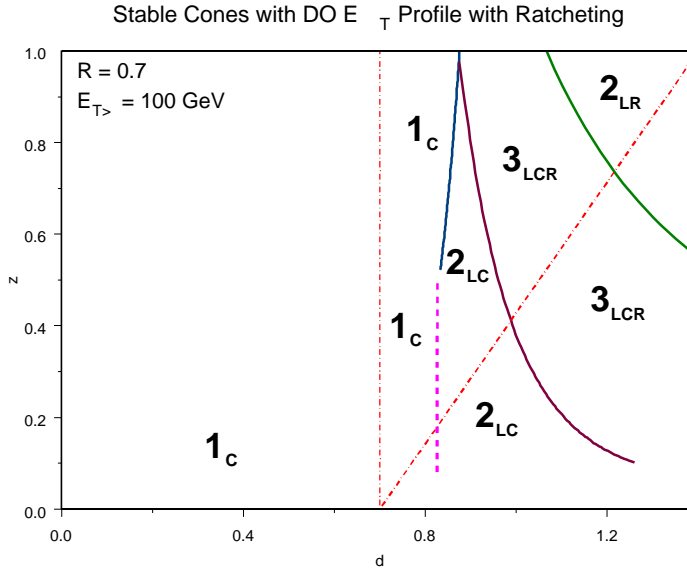
FIG. 14: Gaussian smearing, $\sigma = 0.25$, with ratcheting.

FIG. 15: DØ profile smearing with ratcheting.

z region is essentially unchanged from the no-ratchet case above. However, the 1_L region (both above and below the line $z = (d - R)/R$) is now a 1_C region. The secondary parton is now included in the primary jet, increasing the E_T of the jet and having sizable numerical impact as discussed above. This is even true where we had two jets in NLO (*i.e.*, below the line $z = (d - R)/R$). This is the region where Matthias, in comparing the MidPoint and JETCLU algorithms, uncovered the “lost” jet phenomenon as we expect based on this graphs. It is exactly this lower region in the (d, z) plane that is populated in Matthias’ scatter plots of the location of the “lost” jets (see `z_vs_d_plot_5.ps`). So we do seem to understand the problem. What about the “fix”?

Consider now how the situation changes when we use a smaller cone radius, $R' < R$, while finding the stable cones, but the original R for constructing the jets. The relevant fact, not obvious in the previous graphs, is that the angular structure of the stable cone graphs, approximately scales with the cone radius R , *i.e.*, if we

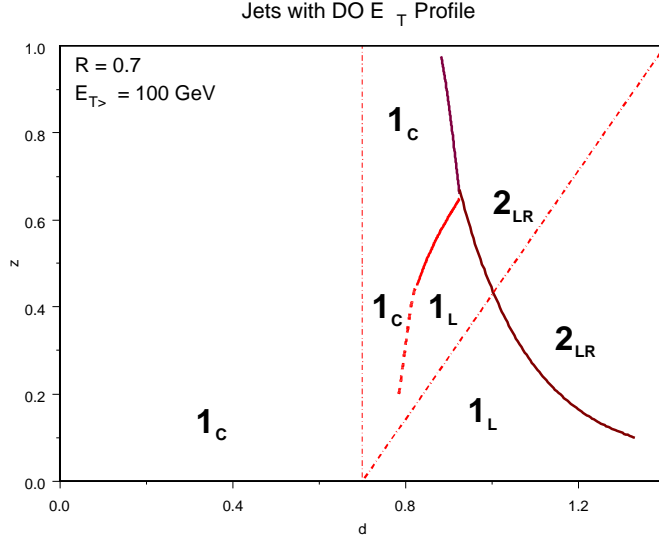


FIG. 16: Found jets in the (d, z) plane with the standard cone algorithm applied to the $D\emptyset$ smearing profile, assuming no central seeds.

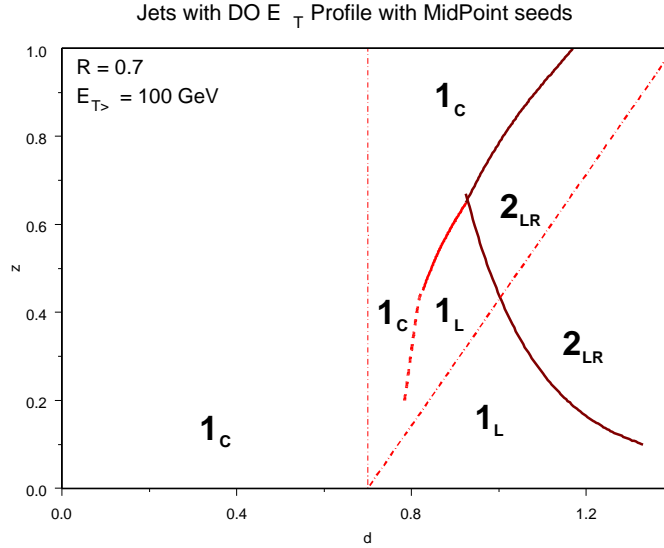


FIG. 17: Found jets in the (d, z) plane with the MidPoint cone algorithm applied to the $D\emptyset$ smearing profile.

plotted versus d/R instead of d , there would be little remaining R dependence. Hence when we perform a stable cone search with, for example, $R' = R/\sqrt{2}$, the structure we have seen above just “slides” to the left (on a fixed d scale) as illustrated in Fig. 19, to be compared to Fig. 16. Note that, in some sense, the situation at large z is actually more different from NLO than in the “unfixed” case. However, as noted earlier this region contains few events and the more important question is what is changing at low z . Here the “fix” tends to convert the previous 1_L region into a 2_{LR} region. Thus the “lost” jet becomes a found jet. However, to fix the jet E_T discrepancy observed by Matthias (*i.e.*, to get closer to the JETCLU result), we need that this found secondary jet be merged with the primary jet. Fig. 19 ignores the issue of merging/splitting by the standard rule, but if we include the expected merging boundary (for $f_{\text{merge}} = 0.5$), we get Fig. In this graph the 2_{LR} region to the left of the dashed merge boundary will be converted to 1_C by the usual merging/splitting rule,

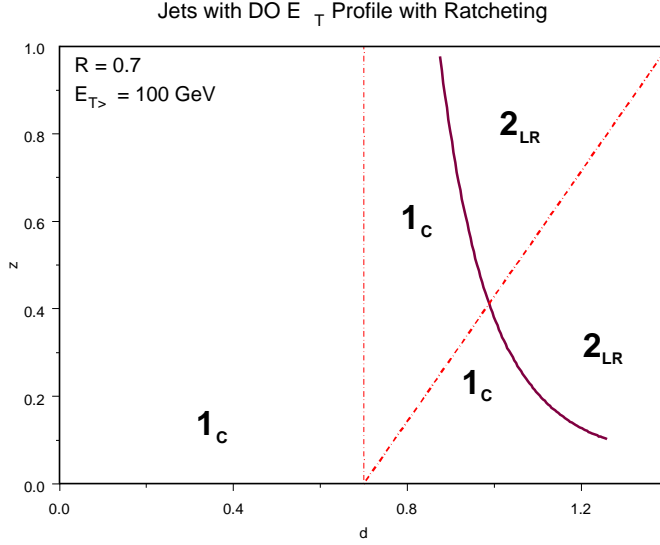


FIG. 18: Found jets in the (d, z) plane with CDF-like cone algorithm with ratcheting applied to the $D\bar{O}$ smearing profile, assuming no central seeds.

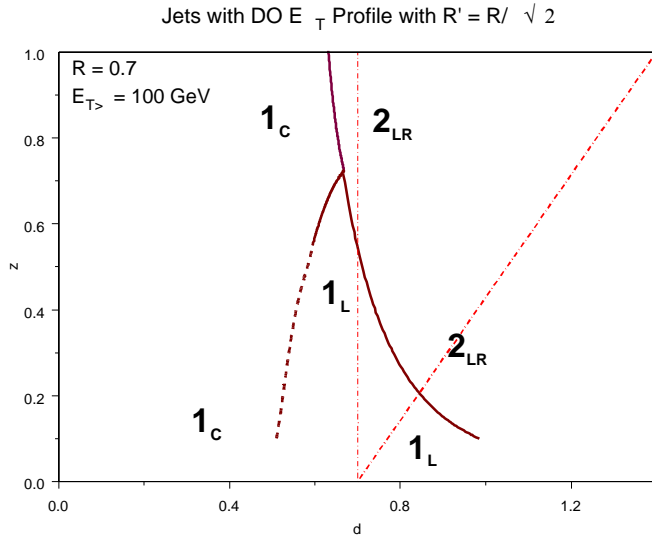


FIG. 19: Found jets in the (d, z) plane with the standard cone algorithm applied to the $D\bar{O}$ smearing profile, assuming no central seeds, but with $R' = R/\sqrt{2}$.

as we want. Thus we can interpret the improvement observed by Matthias with decreasing R' as arising from an increasing region where this conversion occurs. Note that, as we decrease R' , the “lost” jets will slowly disappear from right to left (as the 1_L boundary moves to the left), which is the variation seen in Matthias’ scatter plots noted earlier. So at least qualitatively, this scenario seems to explain Matthias’ plots. (To get things to agree numerically, we probably want the merge rule boundary (the dashed line) to be further to the right, which is just what is suggested in the $D\bar{O}$ note. Maybe I will get that straight eventually).

In summary, the MC data studies by Matthias and the scenario studied analytically here seem to be in reasonable agreement. From my standpoint, the most important outstanding issue is that the current analysis suggests that the R' fix is focused primarily on achieving better agreement with JETCLU exactly in the kinematic region (low z) where JETCLU differs from NLO. Is this a goal we want to achieve, rather than

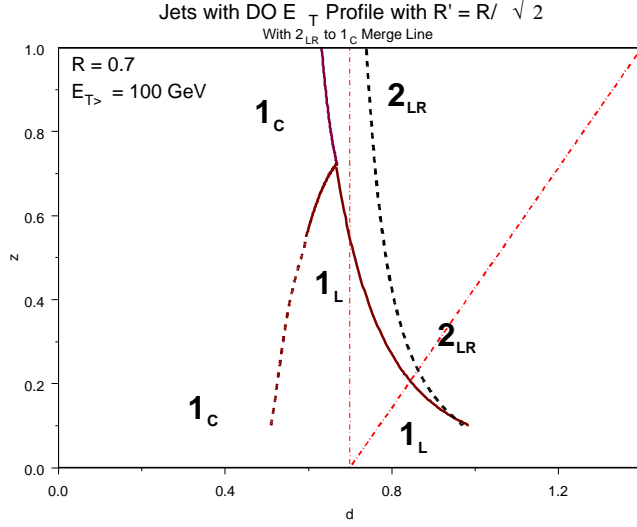


FIG. 20: Found jets in the (d, z) plane with the standard cone algorithm applied to the $D\bar{O}$ smearing profile, assuming no central seeds, but with $R' = R/\sqrt{2}$. The merging boundary is also indicated.

trying to achieve agreement with perturbation theory? Note also that these considerations suggest that the CDF jet cross section, using JETCLU with ratcheting, should be systematically larger than the $D\bar{O}$ jet cross section (with no ratcheting in the jet algorithm). This difference is in addition to the differences in the kinematic variables used in Run I by the two collaborations, which cause the jet cross sections to differ in the same sense. Why don't we see these differences in the published data?